2502 *Chem. Mater.* **2010,** *22,* 2502–2509
DOI:10.1021/cm903404u

CHEMISTRY OF MATERIALS
Article

Interface Energy Measurement of MgO and ZnO: Understanding the Thermodynamic Stability of Nanoparticles

Ricardo H. R. Castro,*,† Ricardo B. Tôrres,‡ Gilberto J. Pereira,§ and Douglas Gouvêa∥

†*Chemical Engineering and Materials Science Department & NEAT ORU, University of California Davis, California 95616,* ‡*Department of Chemical Engineering, and* §*Department of Materials Engineering, FEI University Center, São Bernardo do Campo, SP, 09850-901, Brazil, and* ∥*Department of Metallurgical and Materials Engineering, University of São Paulo, São Paulo, SP, 05508-900, Brazil*

Received November 6, 2009. Revised Manuscript Received March 10, 2010

Nanomaterials have triggered excitement in both fundamental science and technological applications in several fields. However, the same characteristic high interface area that is responsible for their unique properties causes unconventional instability, often leading to local collapsing during application. Thermodynamically, this can be attributed to an increased contribution of the interface to the free energy, activating phenomena such as sintering and grain growth. The lack of reliable interface energy data has restricted the development of conceptual models to allow the control of nanoparticle stability on a thermodynamic basis. Here we introduce a novel and accessible methodology to measure interface energy of nanoparticles exploiting the heat released during sintering to establish a quantitative relation between the solid−solid and solid−vapor interface energies. We exploited this method in MgO and ZnO nanoparticles and determined that the ratio between the solid−solid and solid−vapor interface energy is 1.1 for MgO and 0.7 for ZnO. We then discuss that this ratio is responsible for a thermodynamic metastable state that may prevent collapsing of nanoparticles and, therefore, may be used as a tool to design long-term stable nanoparticles.

Introduction

Most materials exhibit novel physical and chemical properties as their sizes approach nanometer dimensions. This has given rise to the development of several new applications in distinct fields, such as energy, catalysis, sensors, and so forth.[1−3] However, the same nanoscale features that bring the outstanding properties for these materials are also responsible for an increase in the instability of the structures. This instability can cause the collapsing of nanostructures during synthesis, processing, or even during applications, especially when dealing with moderate and high temperatures, which is the case for fuel cells, several gas sensors, and catalysts. To optimize nanoparticles and nanograins and increase their stability, it is important to realize that they are different from bulk materials not only because they are smaller but also because a large fraction of their volume is within the "interface region", that is, a few nanometers or less from the interface itself.[4,5] Thus, nanomaterials properties will be strongly influenced by the interface features, such as composition,[6] structure,[7] stress[8,9] and, fundamentally, energetics.[4,10−12]

The interface energetic is the driving force for phenomena such as sintering and grain growth that are the main phenomena responsible for the nanoparticles collapsing (or controlled processing to obtain fully dense parts). Thermodynamically, they can be expressed as[13,14]

$$\delta G_{sys} = \delta \int \gamma_{SV}\, \mathrm{d}A_{SV} + \delta \int \gamma_{SS}\, \mathrm{d}A_{SS} \qquad (1)$$

where G_{sys} is the total interfacial energy of the system, γ_{SV} and γ_{SS} are the solid−vapor and solid−solid interface energies, respectively, A_{SV} is the specific free surface area (solid−vapor), and A_{SS} is the solid−solid interface area. The first term of this equation is negative because the

*To whom correspondence should be addressed. E-mail: rhrcastro@ucdavis.edu. Fax: (530) 752-9307. Phone: (530) 752-3724.

(1) Seal, S.; Baraton, M. I. *MRS Bull.* **2004**, *29*(1), 9–12.
(2) Messing, G. L.; Stevenson, A. J. *Science* **2008**, *322*(5900), 383–384.
(3) Balaya, P. *Energy Environ. Sci.* **2008**, *1*(6), 645–654.
(4) Navrotsky, A. Thermochemistry of nanomaterials. In *Reviews in Mineralogy and Geochemistry: Nanoparticles and the Environment*; Banfield, J. F., Navrotsky, A., Eds.; Mineralogical Society of America and the Geochemical Society: WA, 2001; Vol. *44*, pp 73−103.
(5) Cao, G.*Nanostructures and Nanomaterials: Synthesis, Properties, and Applications*, 1st ed.; Imperial College Press: Danvers, 2004; p 433.
(6) Castro, R. H. R.; Ushakov, S. V.; Gengembre, L.; Gouvea, D.; Navrotsky, A. *Chem. Mater.* **2006**, *18*, 1867–1872.
(7) Zhao, Z. J.; Meza, J. C.; Van Hove, M. *J. Phys.: Condens. Matter* **2006**, *18*(39), 8693–8706.
(8) Yun, G.; Park, H. S. *Comput. Meth. Appl. Mech. Eng.* **2008**, *197* (41−42), 3337–3350.
(9) Castro, R. H. R.; Marcos, P. J. B.; Lorriaux, A.; Steil, M. C.; Gengembre, L.; Roussel, P.; Gouvea, D. *Chem. Mater.* **2008**, *20*, 3505–3511.
(10) Hill, T. L. *Nano Lett.* **2001**, *1*(3), 111–112.
(11) Hill, T. L. *Nano Lett.* **2001**, *1*(3), 159–160.
(12) Rusanov, A. I. *Russ. J. Phys. Chem.* **2003**, *77*(10), 1558–1563.
(13) Wong, B.; Pask, J. A. *J. Am. Ceram. Soc.* **1979**, *62*(3−4), 138–141.
(14) Liu, F.; Chen, Z.; Yang, W.; Yang, C. L.; Wang, H. F.; Yang, G. C. *Mater. Sci. Eng., A* **2007**, *457*(1−2), 13–17.

 Published on Web 03/30/2010

surface enthalpy is always positive and A_{SV} decreases during both grain growth and sintering, and the second term could be positive during one part of the processes, and negative in another. This is because at some point A_{SV} transforms into A_{SS} by neck formation and, thereafter, A_{SS} rearranges into the bulk structure.[15] Equation 1 shows that nanoparticles are not stable by nature, and collapsing to a micro or macrosize is thermodynamically favorable. However, it also provides the insight that a relatively high γ_{SS} may create an energetic condition where surface elimination is not favorable. That is, since the solid−solid interface must be created during sintering and the $\gamma_{SS}.A_{SS}$ product is not negligible since A_{SS} is inherently high in the nanoscale, it would be possible to put the system in a metastable state, with positive A_{SS} and A_{SV}, where the total collapse of the structure could be avoided during long-term applications. In fact, the concept of metastability in nanoparticles is not new and has been reported by several works in phase transformation studies considering the solid−vapor surface term.[4,6,16−19]

It is important to note that the term $\gamma_{SS}.A_{SS}$ has been neglected in most sintering and grain growth (and phase transformation) discussions because γ_{SS} is considered to be much smaller than γ_{SV} or A_{SS} is too small leading to negligible $\gamma_{SS}.A_{SS}$ product. However, especially for materials with covalent/ionic bonds, such as ceramics, γ_{SS}/γ_{SV} has been reported to be relatively high[20−26] and since the interface area is intrinsically larger in the nanoscale, even low interface energies are expected to contribute significantly to the total free energy of nanoparticles. For instance, in a nanosized powder with 50 m^2 g^{-1}, γ_{SS} as low as 0.5 J m^{-2} accounts for a heat effect of 25 J g^{-1}, which is comparable to the heat of sintering or grain growth.

The lack of experimental thermodynamic data on γ_{SS} for most systems is a drawback for the development of conceptual models for the control of nanoparticles based on thermodynamics. Here we show a novel and convenient methodology for the measurement of average interface energies (meaningful for processing control) by using a standard differential scanning calorimeter (DSC). Using this methodology in selected systems, we show that there is a clear correlation between the interface energies and the observed nanostructure evolution, favoring the metastability hypothesis and indicating that the metastable state can indeed be used as a tool to increase the stability of nanoparticles during application.

Aiming to design the clearest picture of the role of interface energies in the stability of nanoparticles we have chosen two systems with opposite behaviors to conduct the experiments: one that shows relatively stable nanoparticles and nanograins and low sinterability even at high temperatures (magnesium oxide, MgO),[27,28] and another that shows high sinterability with high grain growth even at lower temperatures, with consequent low stability of nanoparticles (zinc oxide, ZnO).[29−31] These are model systems, but there is no reason to believe that the conclusions achieved here are restricted to any particular system.

Interface Energy Measurement

Among the techniques for interface energy measurements reported in the literature, image analysis providing dihedral angle measurements has been used extensively to derive relative energies. This technique, however, has been considered problematic because of surface faceting[32] and also because of the inherent curvature potential that leads to dihedral angle increase.[33] Drop solution calorimetry using dense nanograined ceramics was also proposed as a method to obtain absolute γ_{SS} values.[24] However, the need for spark plasma sintered (SPS) pellets to achieve nanograined sample brings issues related to whether SPS modifies the interface chemistry. Chen and Spaepen[34] explored DSC to extract parameters that characterize the grain growth and used them to derive the surface energy of a metal alloy. Chiang et al.[32] used a similar approach to determine the interface energy of Si and TiO_2. In such an approach, a grain growth model was used and needed a geometric factor accounting for the grain shape and size distribution. After that, Terwillinger and Chiang[35] used DSC to measure the grain boundary energy of TiO_2. Dense nanograined TiO_2 (obtained by HIP) was prepared, and the sintered compact was subjected to heat treatment inside a calorimeter to allow grain growth. The heat released during the process was measured, and the enthalpy related to the interface area decreased, leading to average interface energy. However, the measured heat was small, and the error in the measurement was

(15) Song, X. Y.; Zhang, J. X.; Li, L. M.; Yang, K. Y.; Liu, G. Q. *Acta Mater.* **2006**, *54*(20), 5541–5550.
(16) Levchenko, A. A.; Li, G.; Boerio-Goates, J.; Woodfield, B. F.; Navrotsky, A. *Chem. Mater.* **2006**, *18*, 6324–6332.
(17) Mazeina, L.; Deore, S.; Navrotsky, A. *Chem. Mater.* **2006**, *18*(7), 1830–1838.
(18) McHale, J. M.; Auroux, A.; Perrotta, A. J.; Navrotsky, A. *Science* **1997**, *277*(5327), 788–791.
(19) Pitcher, M. W.; Ushakov, S. V.; Navrotsky, A.; Woodfield, B. F.; Li, G. S.; Boerio-Goates, J.; Tissue, B. M. *J. Am. Ceram. Soc.* **2005**, *88*(1), 160–167.
(20) Tsoga, A.; Sotiropoulou, D.; Nikolopoulos, P. Grain boundary grooving in polycrystalline oxides and surface diffusion coefficient in polycrystalline alumina. In Intergranular and Interphase Boundaries in Materials; Trans Tech Publications: Zurich, Switzerland, **1996**; Vol. *207*, pp 565−568.
(21) Tsoga, A.; Nikolopoulos, P. *J. Mater. Sci.* **1996**, *31*(20), 5409–5413.
(22) Kitayama, M.; Glaeser, A. M. *Key Eng. Mater.* **1999**, *159−1*, 193–204.
(23) Kenway, P. R. *J. Am. Ceram. Soc.* **1994**, *77*(2), 349–355.
(24) Chen, S. S.; Avila-Paredes, H. J.; Kim, S.; Zhao, J. F.; Munir, Z. A.; Navrotsky, A. *Phys. Chem. Chem. Phys.* **2009**, *11*(17), 3039–3042.
(25) Yan, Y.; Chisholm, M. F.; Duscher, G.; Maiti, A.; Pennycook, S. J.; Pantelides, S. T. *Phys. Rev. Lett.* **1998**, *81*(17), 3675–3678.
(26) Broqvist, P.; Gronbeck, H.; Panas, I. *Surf. Sci.* **2004**, *554*(2−3), 262–271.
(27) Gupta, T. K. *J. Mater. Sci.* **1971**, *6*(1), 25–&.
(28) Kleiman, S.; Chaim, R. *Mater. Lett.* **2007**, *61*, 4489–4491.
(29) Auffredic, J. P.; Boultif, A.; Langford, J. I.; Louer, D. *J. Am. Ceram. Soc.* **1995**, *78*(2), 323–328.
(30) Gupta, T. K.; Coble, R. L. *J. Am. Ceram. Soc.* **1968**, *51*(9), 521–525.
(31) Sabioni, A. C. S. *Solid State Ionics* **2004**, *170*(1−2), 145–148.
(32) Chiang, Y.-M.; Smyth, I. P.; Terwillinger, C. D.; Petuskey, W. T.; Eastman, J. A. *Nanostruct. Mater.* **1992**, *1*, 235–240.
(33) Chiang, Y.-M.; Birnie, D.; Kingery, W. D. *Physical Ceramics - Principles for Ceramic Science and Engineering*; John Wiley & Sons Inc.: New York, 1997.
(34) Chen, L. C.; Spaepen, F. *J. Appl. Phys.* **1991**, *69*(2), 679–688.
(35) Terwillinger, C. D.; Chiang, Y.-M. *J. Am. Ceram. Soc.* **1995**, *78*(8), 2045–2055.

considerably high. Here we propose for the first time a method based on DSC of nanosized powders subjected to sintering. The objective is to determine a relationship between the γ_{SV} and γ_{SS} by correlating the measured enthalpy during sintering and the microstructure changes occurring during the process, avoiding the use of arbitrary coarsening models. The use of nanoparticles is necessary to increase the energy released during the process and make it measurable.

When sintering is carried out inside DSC equipment, there may be several heat effects caused by the various mass transport mechanisms,[27,33] providing a complex overlap of signals. However, a good microstructural characterization of arbitrarily chosen initial and final states can be used to derive interface energies. The path by which the transformation occurs is, therefore, unimportant, since the final and initial states will have an energetic difference given by the DSC peak integral. Considering the sintering of a polycrystalline nanosized powder, the energy of two subsequent states (#1 and #2) of a sample subjected to sintering can be described as:

$$State\ \#1: \qquad A_{SV(1)} \times \gamma_{SV} + H_B + A_{SS(1)} \times \gamma_{SS} \quad (2)$$

$$State\ \#2: \qquad A_{SV(2)} \times \gamma_{SV} + H_B + A_{SS(2)} \times \gamma_{SS} \quad (3)$$

where H_B is the bulk enthalpy, that is assumed to remain unchanged during sintering, and subscripts 1 and 2 indicate the respective states. Therefore, the measured enthalpy during sintering of the sample will be obtained by subtracting eq 3 and 2. An accurate measurement of A_{SV} and A_{SS} in both states will provide a relationship between γ_{SV} and γ_{SS}. A_{SV} can be determined by gas adsorption methods (BET), A_{SS} can be estimated by comparing the specific surface area measured by gas adsorption and the interface area calculated from the crystallite size[36] (A_{CS}) measured by X-ray diffraction analysis (Scherrer method[37]). If the particle sizes cannot be reliably estimated by the Scherrer approach, a quantitative microscopy analysis is necessary.

The possibility must be considered that the adopted DSC measurement is affected by another heat exchanging process occurring simultaneously to sintering. This includes any phase transformation, relief of lattice strain, oxidation/reduction, and desorption of gases (including physisorbed and chemisorbed water and carbon dioxide). These extraneous contributions can be controlled by adopting special experimental and sample conditions to decrease their heat contribution to a negligible amount.[35] The major problem is the significant amount of water on the surface. This is particularly large for nanosized powders (needed for these experiments, because the specific surface areas need to be high). To account for the heat of H_2O released during sintering, one can measure the mass

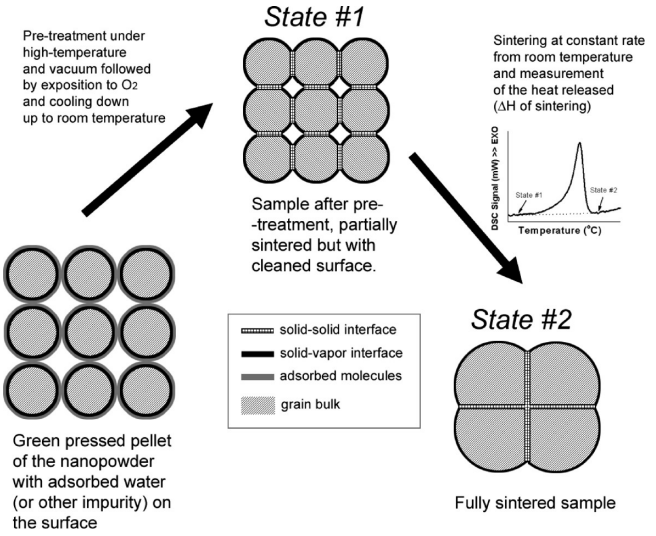

Figure 1. Schematic representation of the microstructure of the nanosized powder during the calorimetric procedure to measure interface energy. In the procedure, the powder is compacted using high uniaxial pressure. At this point, the particles have adsorbed water and strain due to compaction. The sample is then treated under vacuum ($\sim 10^{-4}$ Torr) and enough high temperature to clean the surface from impurities (pre-treatment). The microstructure after pre-treatment has already some neck formation since sintering is unavoidable, but still enough area to be measured (State #1). Still in the pre-treatment, sample is exposed to O_2 to allow reoxidation and is slowly cooled down inside the instrument chamber to allow tension relaxation. Finally, the sample is subjected to sinter, and the DSC signal is measured. The microstructure evolution (from State #1 to State #2) shows both surface and grain boundary area changes that will be correlated with eqs 3 and 2 and the measured enthalpy.

of H_2O difference between states #1 and #2 and use the data to calculate the total energy of desorption using the negative of the H_2O adsorption enthalpy.[6,38] However, the amount of adsorbed H_2O may change the surface energy of oxides in a "curing" effect.[18] The extent of this change depends on the H_2O amount, which is variable during sintering. To decrease the effect of water during sintering, we propose a pre-treatment of the samples inside the DSC to dry and clean the samples from water, carbonates, and other contaminants (minimizing their energetic effects). This is achieved through a thermal treatment under vacuum (10^{-4} Torr) at a relatively high temperature, chosen to remove water and carbonates but to minimize sintering. After treatment, the sample is slowly cooled inside the DSC instrument under oxygen (to provide reoxidation of surface and strain relief), and sintered without taking the sample out of the analysis chamber. Figure 1 shows a flowchart indicating the basic steps of the DSC sintering experiment highlighting the microstructure during each stage.

Note that in this procedure we assume that the surface energy in the nanosized crystals and in their bulk counterparts are the same, and also that the surface energy is not drastically affected by the temperature. In fact, an extension of Gibbs thermodynamics may show that the surface energy of spherical particles decreases as the radius decreases.[39] This behavior is expected in isotropic

(36) Radha, A. V.; Bomati-Miguel, O.; Ushakov, S. V.; Navrotsky, A.; Tartaj, P. *J. Am. Ceram. Soc.* **2009**, *92*(1), 133–140.
(37) Cullity, B. D., *Elements of X-ray Diffraction*, 2nd ed.; Addison-Wesley Publishing Company: MA, 1978.
(38) Ushakov, S. V.; Navrotsky, A. *Appl. Phys. Lett.* **2005**, *87*(16), 164103.
(39) Buff, F. P. *J. Chem. Phys.* **1951**, *19*(12), 1591–1594.

particles such as relatively low melting point metals. When dealing with anisotropic ceramic nanoparticles, with highly directional and strong bonds, the effect of the size on the surface energy is expected to be smaller since atoms tend to be mostly oriented by the crystalline structure. In very small nanosized samples (< 5 nm), perhaps a higher degree of disorder may affect the surface energy, and those samples should be avoided in the proposed approach. The effect of temperature may also be neglected in the surface energy as predicted by Shebzukhova et al.[40] Their work predicts that the surface energy for high temperature metals may vary by only ~0.03 mJ m^{-2} K^{-1} (data for Thorium). However reported data could not be found in the literature for oxides, a similar trend can be expected (~0.001 J m^{-2} for 400 K of temperature difference) and is negligible since it is within the error of our proposed analysis.

Experimental Procedures

MgO and MgO 0.5 mol % CaO samples were synthesized by using the liquid precursor method. A 145 g portion of citric acid was mixed with 105 mL of ethylene glycol, and the mixture was heated up to 110 °C under stirring until total dissolution. A 53 g portion of magnesium acetate was then introduced in the solution with 120 mL of deionized H_2O. The mixture was heated up to 145 °C for polyesterification and formation of chelates between Mg^{2+} (and Ca^{2+}) and carboxyl groups. The resin was treated at 450 °C for 4 h, and the resulting carbon-rich powder was ground in a mortar. The ground powder was then treated at 600 °C for 15 h in air to burn the remaining organic material. High-purity ZnO nanoparticles were purchased from Sigma-Aldrich. X-ray diffraction measurements (XRD) were carried out using D8 Advance Bruker with 0.05° and exposure time of 5 s (Cu Kα radiation, incident beam monochromator). Specific surface area of the powder was measured by gas adsorption using a Micromeritic Gemini 2375 instrument after treating the sample at 300 °C under vacuum for 10 h. Grain boundary area was estimated by the difference between the interface area calculated from crystallite size measured by XRD (JADE 6 XRDWS − Materials Data, Inc.) and surface area measured by gas adsorption.[36] DSC experiments were conducted in a Setsys Evolution 18 DSC/TG, Setaram Inc. (DSC sentitivity 0.4 μW and TG resolution 0.03 μg). Three pellets with final diameter of 3 mm (50 mg each) were used in each of the three experiments conducted for the interface energy measurement. Compaction of pellets were conducted using an uniaxial pneumatic press - TOK Pressotechnik with precision > 0.1%. SEM was conducted in a FEI Quanta FEG operated at 10 kV and high vacuum. Crystallite sizes and interface areas from SEM image analysis were consistent with those measured by gas adsorption and XRD pattern analysis. Microprobe analysis were carried out using Cameca SX-100 electron probe microanalyzer, with accelerating potential 15 kV, beam current ~10 nA, and peak and background count times of 10 s.

Results and Discussion

Figure 2 shows the experimental heat released during sintering of a nanosized powder of MgO measured using DSC. In this procedure, high purity synthesized nano MgO (> 99.99%) was pressed into pellets (70 Kgf mm^{-2}) to imply maximum particle contact (to maximize sintering kinetics and sharpen heat peaks), pre-treated at 950 °C under vacuum for 30 min and exposed to O_2 (to avoid reduction effects) and slowly cooled down inside the DSC chamber. After that, we submitted the sample to scanning sintering conditions using heating rate at 20 °C min^{-1}. An experimental baseline was carried out using pre-sintered MgO pellets (1600 °C for 4 h) using the same routine and subtracted from the sintering DSC data. Other temperatures for pre-treatment (500, 600, and 700 °C) were tested but mass changes during sintering were too large for the lower temperatures, indicating residual absorbed agents. The figure shows the already corrected exothermic peak when the system evolves from State #1 (at 950 °C) to State #2 (1300 °C), as identified in the figure. This is just a representative curve since three experiments were carried out for each sample to ensure repeatability and estimate deviation.

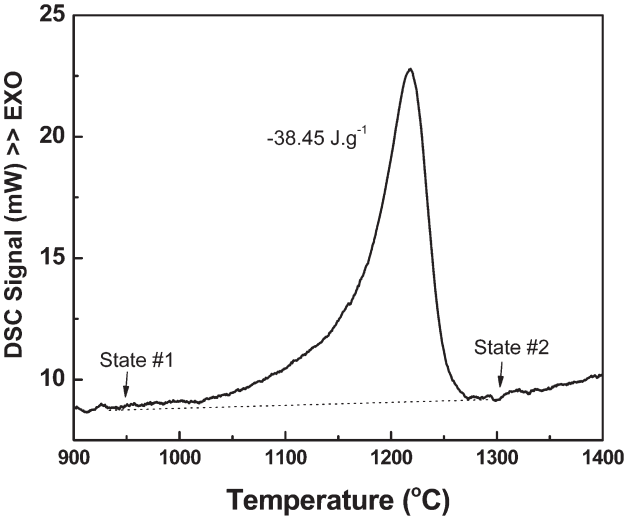

Figure 2. Trace of DSC curve for MgO nanosized powder pelletized under high pressure and sintered at 20 °C.min^{-1}. States #1 and #2 indicate the initial and final stages of the sintering, respectively. The enthalpy measured was −38.45 J g^{-1}. The peak starts only at 950 °C because the samples were pre-treated at 950 °C under vacuum to eliminate adsorbed molecules, such as water and carbon dioxide.

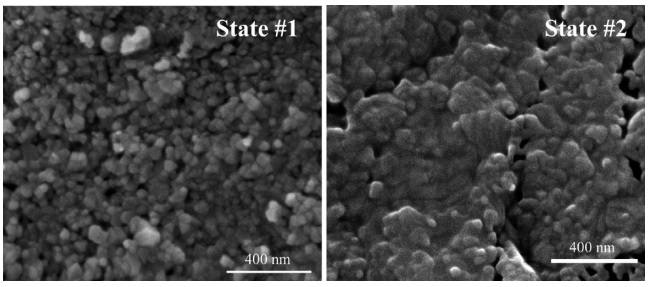

Figure 3. SEM micrographs of MgO samples quenched from 950 °C (State #1) and 1300 °C (State #2). Nanosized particles are observed in both states. Neck formation as an evidence for sintering is observed in State #2. The energy released during this process (Figure 2) can be attributed to the interface area evolution, leading to a correlation between γ_{SS} and γ_{SV}.

The microstructure evolution during this process can be observed in Figure 3 by the SEM of the MgO pellets

(40) Shebzukhova, I. G.; Aref'eva, L. P.; Khokonov, K. B. *Phys. Met. Metallogr.* **2008**, *105*(4), 338–342.

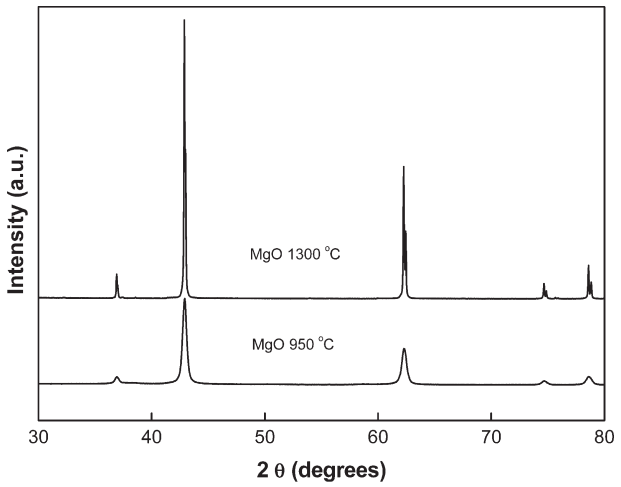

Figure 4. XRD diffraction patterns for MgO nanosized powder pelletized and subjected to sintering. Both temperatures show the same periclase MgO structure. There is no evidence of second phases, segregation, phase or transformation during the sintering process. This is consistent with the SEM and microprobe analysis.

rapidly quenched from states #1 and #2 to room temperature. It shows sintering, with neck formation, grain growth, and moderate pore elimination. Using X-ray diffraction, only MgO with periclase structure was detected in both states (Figure 4), so the heat released could be assigned to the sintering process. Microprobe analysis showed no modification in composition during this process or segregation of impurities. Negligible strain was observed in the sample treated at 950 °C (0.073%) and at 1300 °C (~0.000%). Thermogravimetric data recorded during this process showed a weight change of 0.011%, which is negligible and reveals the effectiveness of the pre-treatment.

Combining the measured enthalpy (-38.4 ± 1.4 J g^{-1}) and the quantified microstructure characterization shown in Table 1, the following equation relating the interface energy emerges:

$$51.1\ \mathrm{m^2\ g^{-1}}\cdot\gamma_{SV} - 13.3\ \mathrm{m^2\ g^{-1}}\cdot\gamma_{SS} = 38.4\ \mathrm{J\ g^{-1}} \quad (4)$$

From this, $\gamma_{SS} = 1.2 \pm 0.5$ J m^{-2} can be derived by using the surface energy data reported by Tasker[41] (1.1 J m^{-2}). This energy is consistent with previously reported data from other techniques[42,43] and, as expected, is higher than the surface energy.

Figure 5 shows the heat released during sintering of nanosized ZnO particles. In this procedure, high purity ZnO was pressed into pellets (70 Kgf mm^{-2}) and heated at 20 °C.min^{-1}, similarly to MgO. The pre-treatment was carried out under vacuum at 550 °C to avoid extreme coarsening of the sample that could make unviable the following sintering procedures. Other temperatures (350, 450, and 700 °C) were tested for the pre-treatment but mass changes during sintering were too large for the lower temperatures, and coarsening was too severe for the higher one. The microstructures of the samples in State #1 (550 °C) and State #2 (1350 °C) are shown in Figure 6 and Table 1, and it is evident that pronounced grain growth takes place during sintering. This is consistent with the broader and doubled heat effect in DSC measurement, representing the heat of both processes taking place. Negligible strain was observed in the sample treated at 550 °C (0.017%) and at 1400 °C (−0.021%). Note that despite the high temperature of State #2, no significant mass loss was observed during the experiment (0.040%), showing that there was no significant evaporation of the sample during sintering. This can be attributed to the relatively high heating rate used in the experiment. The measured enthalpy was -26.7 ± 6 J g^{-1}, and the following equation was derived from the data presented in Table 1:

$$2.5\ \mathrm{m^2\ g^{-1}}\cdot\gamma_{SV} + 11.7\ \mathrm{m^2\ g^{-1}}\cdot\gamma_{SS} = 26.7\ \mathrm{J\ g^{-1}} \quad (5)$$

Hence, $\gamma_{SS} = 1.8 \pm 0.4$ J m^{-2} can be calculated using the surface energy data reported by Xu et al. (2.5 J m^{-2}).[44] This result is also consistent with the literature available data for the grain boundary energy in ZnO,[45] and shows that it is significantly lower than the surface energy in this case. Note that in this case, the interface areas after sintering are considered negligible. In fact, the reliability of the interface area measurements used here in samples with relatively too large (or small) particle sizes is very limited. However, this inaccuracy will not significantly affect the calculated energies in this particular case. This is because the measured heat is associated with the interface area variation. In the studied case the interface area after pre-treatment is much higher than after sintering, such that the final interface area will not significantly affect the final numbers. For instance, SEM of the after sintering sample indicates a particle size of 2−100 μm. This corresponds to a solid−solid area varying from 0.2 to 0.005 m^2 g^{-1}. Since the initial A_{SS} is 11.7, the area variation would be in the range 11.5−11.7 m^2 g^{-1}. If this is considered zero (as used in our calculations), the results would differ only by 0.02 J m^{-2}, which is within the standard deviations.

Observing and comparing the results for interface energies of MgO and ZnO (Table 1), one may note that the ratio between the γ_{SS} and γ_{SV} for each oxide is considerably different ($\gamma_{SS}/\gamma_{SV} = 1.1$ for MgO and 0.7 for ZnO). Moreover, the observed SEM micrographs reveal that MgO retains nanograins even at temperatures as high as 1300 °C, while ZnO does not. These results are very consistent with the metastability hypothesis developed from eq 1, where the term $\gamma_{SS}.A_{SS}$ may create an energy barrier for sintering. That is, as the grains grow the contribution of $\gamma_{SV}.A_{SV}$ decreases and that of $\gamma_{SS}.A_{SS}$

(41) Tasker, P. W. Surfaces of magnesia and alumina. In *Advances in Ceramics*; Kingery, W. D., Ed.; American Ceramic Society: Columbus, OH, 1984; Vol. *10*, pp 176−189.
(42) Harris, D. J.; Harding, J. H.; Parker, S. C. *Radiat. Eff. Defects Solids* **1999**, *151*(1−4), 299–304.
(43) Kinderlehrer, D.; Ta'asan, S.; Livshits, I.; Mason, D. E. *Interface Sci.* **2002**, *10*(2−3), 233–242.
(44) Xu, F.; Zhang, P.; Navrotsky, A.; Yuan, Z.-Y.; Ren, T.-Z.; Halasa, M.; Su, B.-L. *Chem. Mater.* **2007**, *19*, 5680–5686.
(45) Sato, Y.; Mizoguchi, T.; Oba, F.; Ikuhara, Y.; Yamamoto, T. *Phys. Rev. B* **2005**, *72*, 064109.

Table 1. Interface Areas for MgO, ZnO and Doped MgO at Reference States #1 and #2 during Sintering Experiment and Respective Derived Interface Energies[a]

	interface areas ($m^2\ g^{-1}$)					
	State #1		State #2		interface energies ($J\ m^{-2}$)	
	SV	SS	SV	SS	SV	SS
MgO	59.3 ± 2.0	~0	8.2 ± 0.5	13.3 ± 2.5	1.07[41]	1.2 ± 0.2
ZnO	2.5 ± 0.5	11.7 ± 2.5	~0	~0	2.55[44]	1.8 ± 0.4
MgO 0.5% CaO	43.7 ± 2.0	15.7 ± 2.0	~0	1.2 ± 1	0.6[52]	0.4 ± 0.2

[a] The surface (solid-vapor) energy data are from the literature as indicated. SV and SS are abbreviations for solid−vapor and solid−solid interfaces.

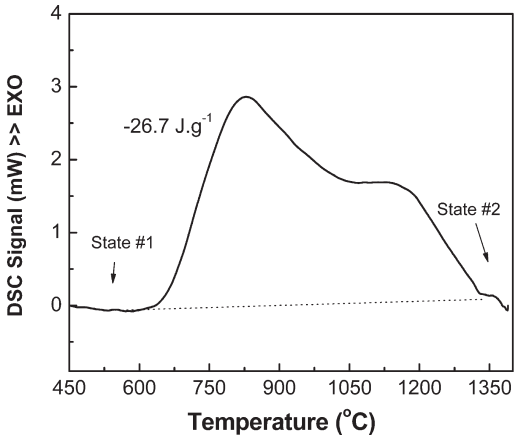

Figure 5. Trace of DSC curve for ZnO nanosized powder pellets under sintering. States #1 and #2 indicate the initial and final stages of the sintering, respectively. The enthalpy measured was $-26.7\ J\ g^{-1}$. The heat effects start only after 550 °C because the samples were pre-treated at this temperature under vacuum to eliminate adsorbed molecules, such as water and carbon dioxide. At least two peaks can be identified; one is attributed to initial stage of sintering, with neck formation, and the other is attributed to grain growth that is very pronounced in ZnO. This data was used to calculate the interface energies for ZnO.

increases in the initial stages. This last increases the energy cost for surface elimination, creating a metastable state, and, the higher the γ_{SS}/γ_{SV} ratio, the higher the energy well created.

Simulations of sintering have shown this effect of the solid−solid interface energy in limiting densification during ceramic processing (in a similar approach to the nanoparticle stability study).[44,45] However, since the simulations are usually restricted to two particles or small clusters (to limit simulation time), the effect of the solid−solid interface energy in the total energy may be underestimated. That is, if one considers a two particles problem, the surface area is always geometrically higher than the grain boundary. In an infinite number of particles problem, the grain boundary area can be comparable to the surface area in the first stages of sintering (especially when sintering nanoparticles), and with a relatively high solid−solid interface energy, the metastability hypothesis could be seen from simulations. We expect that our work will stimulate more complex simulations of sintering and grain growth using large clusters and using γ_{SS}/γ_{SV} higher than unity.

To further test the metastability hypothesis, we searched the literature and cross data related to sinterability and interface energy. We observed that several materials with high γ_{SS}/γ_{SV} (when data is available), such

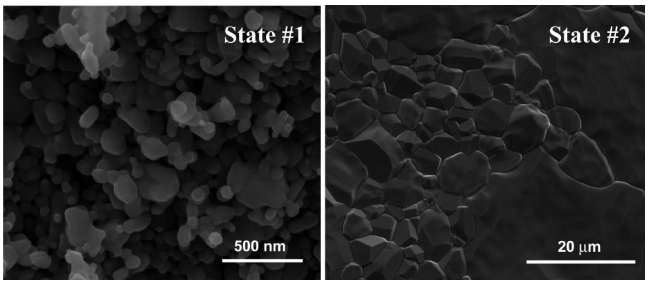

Figure 6. SEM micrographs of ZnO samples quenched from 550 °C (State #1) and 1350 °C (State #2) during similar sintering procedures used in the DSC experiment. Nanosized particles are observed in State #1. Pronounced grain growth was observed in the sample during sintering, and State #2 shows microsized grains. The energy released during this process (Figure 5) can be attributed to the interface area evolution, leading to a correlation between γ_{SS} and γ_{SV}.

as Al_2O_3 (0.9−1.6[46]), SiC (1.2[47]), ZrO_2 (1.3−1.7[48]), and others, also show low densification during sintering and higher stability of nanoparticles. Moreover, dopants prone to form surface excess change this behavior, since they directly affect the interface energetics. Furthermore, these pure materials easily agglomerate after synthesis or during sample preparation (typically seen in HRTEM of nanoparticles and from discrepancies between interface areas calculated from the XRD diffraction and gas adsorption analysis). The formation of these strong agglomerate interfaces (grain boundary like) could be occurring because of bringing relative stability to the nanoparticle throughout the metastable condition. On the other hand, materials with low γ_{SS}/γ_{SV} show instability and high sinterability, as with most metallic alloys.[49]

The metastability hypothesis could be confronted using a kinetic approach arguing that the observed instability of ZnO (and similar materials) lies on its high diffusion coefficient, which is considerably higher than that of MgO at the same temperature (even when normalized with the melting point). This possibility can be analyzed by comparing the stability results of MgO with a system with similar diffusion coefficient. For instance, MgO doped with 0.5% of CaO was subjected to the same DSC experiment to measure the interface energy. Figure 7 shows the DSC measured signal, and Figure 8 shows the respective SEM micrograph for states #1 (950 °C) and #2

(46) Handwerker, C. A.; Dynys, J. M.; Cannon, R. M.; Coble, R. L. *J. Am. Ceram. Soc.* **1990**, *73*(5), 1371–1377.
(47) Gubernat, A.; Stobierski, L. *Ceram. Int.* **2003**, *29*(8), 961–965.
(48) Shibata, N.; Yamamoto, T.; Ikuhara, Y.; Sakuma, T. *J. Electron Microsc.* **2001**, *50*(6), 429–433.
(49) Kudrman, J.; Cadek, J. *Czech. J. Phys.* **1969**, *19*(11), 1337.

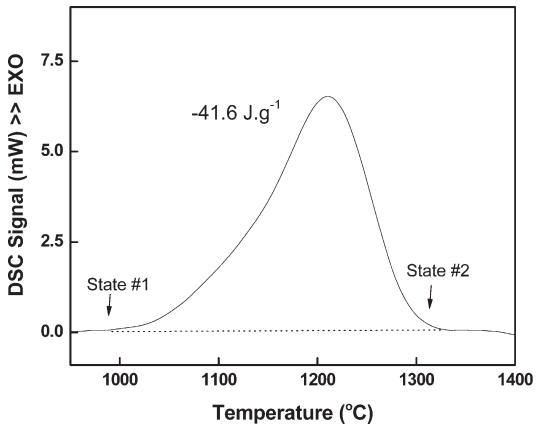

Figure 7. Trace of DSC curve for MgO doped with 0.5 mol % of CaO nanosized powder pellets under sintering. States #1 and #2 indicate the initial and final stages of the sintering, respectively. The enthalpy measured was -41.6 J g^{-1}. As occurred for pure MgO, the peak starts only at 950 °C because the samples were pre-treated at 950 °C under vacuum to eliminate adsorbed molecules, such as water and carbon dioxide.

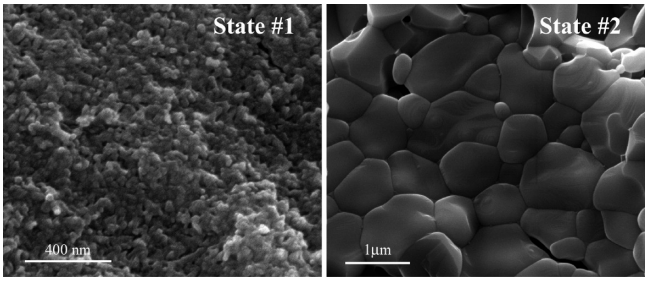

Figure 8. SEM micrographs of MgO doped with 0.5 mol % of CaO samples quenched from 950 °C (State #1) and 1300 °C (State #2) during similar sintering procedure used in the DSC experiment (Figure 1). Nanosized particles are observed in State #1. Pronounced grain growth was observed in the sample during sintering and State #2 shows micro-sized grains. This is very similar to the ZnO behavior despite the pronounced difference in the diffusion parameters. The energy released during this process can be attributed to the interface area evolution, leading to a correlation between γ_{SS} and γ_{SV}, which was more similar to that for ZnO than for pure MgO.

(1300 °C). Negligible strain was observed in the sample treated at 950 °C (0.010%) and at 1300 °C (~0.000%). The microstructure observed in State #2 was similar to that of ZnO in the same state despite the temperature difference, showing pronounced grain growth. However, the diffusion in this compound is not expected to be considerably higher than that of pure MgO since Ca^{2+} has the same valence of Mg^{2+}, and the ionic radius difference is not big. The explanation for the observed results must lie in the effect of Ca^{2+} in the interface energy of MgO. In fact, CaO is observed to spontaneously segregate to the interface of MgO,[50,51] leading to an interface energy decrease.[52] The measured ratio here was $\gamma_{SS}/\gamma_{SV} = 0.67$ (see Table 1), reinforcing the metastability hypothesis and demonstrating the possibility of manipulation of the interface energies using small amounts of dopants prone to segregate on the interfaces.

A perhaps contradictory data appears when observing the increase of A_{SS} after sintering for pure MgO, a different trend comparing with the other two systems of ZnO and doping MgO (Table 1). That is, since γ_{SS} is relatively higher for pure MgO, one could immediately expect a lower area to be formed in the metastable state. However, deeply analyzing the data, one observes that the formation of the interface area is also observed for doped MgO and ZnO, but in those cases it appears already during the pre-treatment. The interface areas for ZnO and doped MgO rapidly vanish during subsequent sintering, but for MgO it does not. This phenomenon is not directly related to the mentioned metastable state, but to the local thermodynamics of grain boundary elimination during sintering, which is highly dependent on the dihedral angle. That is, whenever the solid−solid interface energy is relatively low, the equilibrium angle is high, and the mass centers of the grains will naturally approach during sintering, leading to fast grain boundary elimination. If γ_{SS} is relatively high, the dihedral angle is low, and the neck will form only until this angle is achieved. In this case, the centers of the grains won′t get too close, otherwise the angle would change, disrespecting the local thermodynamics. This fixed angle is seen as sintering with high grain growth, which is well seen in MgO and not in doped MgO or ZnO.

Conclusion

We showed that one is capable of measuring the average interface energy using a regular DSC instrument. This was possible because of the inherent high surface area of nanoparticles that allows measurable heat of sintering during DSC. Although the work was focused in ceramic powders, metallic nanoparticles should also be suitable, but because of the inherent lower solid−solid interface energy, only surface energy will be derived.

The new calorimetric methodology is, however, highly dependent on the characterization of the interface areas. The technique used in this work for determination of interface area (solid−solid) after sintering is not very reliable when dealing with very small particles. Although this may not present issues when calculating energy changes for systems with large amount of grain growth (as in ZnO), it could cause large errors when calculating energy changes in systems with very little grain growth (as MgO), since the solid−solid interface area is not negligible and accounts for a larger portion in the overall energy changes.

The measured data combined with some literature reports were used to develop a hypothesis of metastability of nanoparticles that can be used to predict the stability of nanostructures in relatively high temperature applications. The effect of Ca^{2+} in the interface energy opens a great perspective for controlling the stability of nanoparticle not by diffusion but by using thermodynamics, that is, controlling of interface energies using dopants. The

(50) Tasker, P. W.; Colbourn, E. A.; Mackrodt, W. C. *J. Am. Ceram. Soc.* **1985**, *68*(2), 74–80.
(51) Millett, P. C.; Selvam, R. P.; Saxena, A. *Acta Mater.* **2007**, *55*, 2329–2336.
(52) Duffy, D. M. *J. Phys. C: Solid State Phys.* **1986**, *19*, 4393–4412.

hypothesis is applicable even during synthesis in a liquid medium, but in this case one must consider that there is a solid−liquid interface rather than solid−vapor, with a different energy, and that this energy may be affected by any surfactant agent.

Acknowledgment. The University of California Davis is acknowledged for start up funds. The Brazilian agency FAPESP is acknowledged for the financial support. The FEI University Center is acknowledged for providing the infrastructure for part of the study. TLJC.